On the solution of the full three-dimensional Taylor bubble problem by using a coupled Conservative Level Set - Moving Mesh method

On the solution of the full three-dimensional Taylor bubble problem by using a coupled Conservative Level Set - Moving Mesh method

E Gutiérrez[1], N Balcázar[1], O Lehmkuhl[1,2] and A Oliva[1]

[1] Heat and Mass Transfer Technological Centre (CTTC), Universitat Politècnica de Catalunya (UPC), ESEIAAT, Carrer de Colom 11, 08222 Terrassa (Barcelona), Spain.
[2] Termo Fluids S.L., Avinguda de Jaquard, 97 1-E, 08222 Terrassa (Barcelona), Spain.

E-mail: cttc@cttc.upc.edu

Abstract. The challenging problem of the full three-dimensional Taylor bubble has been addressed by using a Conservative Level Set method in order to deal with the multiphase flow. A moving mesh is used, aiming to optimize the simulation domain. The mesh is moved as the bubble rises, so the region of study can be limited to the surroundings of the bubble, notably reducing the domain's size. This saving in the computational resources facilitates to face the Taylor bubble problem without the axisymmetric assumption. By doing so, a detailed description of the fluid field is provided, comparing the results against numerical and experimental data.

1. Introduction

The slug flow is of great importance in a broad range of technological applications and natural phenomena: heat transport systems, chemical reactors, blood flow, etc. In order to completely understand this kind of flow, the fundamental problem of a single Taylor bubble should be deeply comprehended. The study of these bubbles started with the publications of Davies and Taylor [1] and White and Beardmore [2]. Since then, several approaches have been assessed to study Taylor bubbles, both experimental and numerical (see for instance [3, 4]).

The present paper propose a new coupled Conservative Level-Set - Moving Mesh method to solve the Taylor bubble problem. On the one hand, the employed Conservative Level-Set method (CLS) was developed by Balcázar et al. [5], in the framework of finite-volume discretizations and unstructured meshes. On the other hand, by using a moving mesh, the intention is to optimize the simulation domain.

Buoyant bubble problems need the use of large domains to achieve proper capture of the phenomena. That is due to the need of leaving enough vertical space for the bubble to reach its steady state. Indeed, much of the domain is not of direct relevance in the study of the bubble's dynamics, causing the loss of computational efficiency in the calculation process. The region of interest includes the bubble, its proximities and its wake. Areas far from the bubble are not relevant, since the fluid remains stagnant. To tackle this issue, different approaches have been proposed in the literature: methods based on periodic boundaries and a fringe zone that damps the wake of the bubble [6, 7]; methods based on attaching a new non-inertial reference frame to

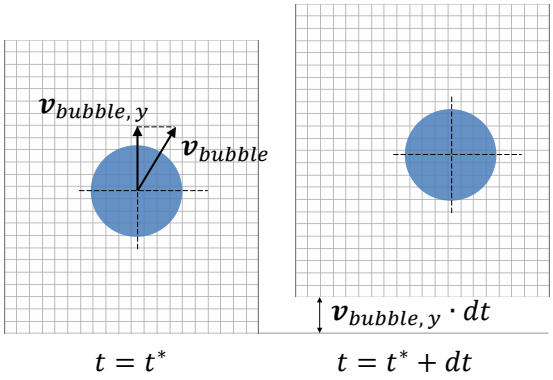

Figure 1. Moving mesh method representation, showing two consecutive time instants.

the bubble centroid [8, 9], and methods based on dynamic meshes [10, 11]. We chose this last technique to optimize the simulation domain within the CLS framework.

Using the aforementioned method, the well-known experiment of Bugg and Saad [12] has been numerically studied. Results have also been compared against other numerical simulations [13].

2. Governing equations and Numerical method

Assuming multiphase incompressible flow, Newtonian fluids, dynamic mesh, no mass transfer at the interface between fluids and constant surface tension coefficient σ, the Navier-Stokes equations governing the fluid motion are given by the conservation laws for momentum and mass shown below:

$$\frac{\partial}{\partial t}(\rho \mathbf{v}) + \nabla \cdot (\rho \mathbf{v}(\mathbf{v} - \mathbf{v}_{\text{mesh}})) = -\nabla p + +\nabla \cdot \mu \left(\nabla \mathbf{v} + (\nabla \mathbf{v})^T\right) + \rho \mathbf{g} + \sigma \kappa \mathbf{n} \delta_\Gamma + \Psi_{\rho_0} \tag{1}$$

$$\nabla \cdot \mathbf{v} = 0 \tag{2}$$

where t is the time, ρ and μ are respectively the fluid density and viscosity, $\mathbf{v}$ is the velocity field, $\mathbf{v}_{\text{mesh}}$ is the mesh velocity (which for this specific case is identical to the vertical component of the bubble velocity), p is the pressure field, $\mathbf{g}$ is the gravity acceleration, $\mathbf{n}$ is the unit normal vector to the interface, κ is the interface curvature, δ_Γ is the Dirac delta function located at the interface, and $\Psi_{\rho_0} = -\rho_0 \mathbf{g}$ represents an extra source term needed to compensate the weight of the fluids within the domain [14, 15]. Figure 1 shows how the dynamic mesh works in this model. The mesh is moving at the vertical velocity of the bubble, so ostensibly the bubble remains vertically stationary inside the domain.

The two major challenges of simulating fluid interfaces are to maintain a sharp front and to compute the surface tension accurately [16]. In order to deal with this issues, the CLS method implemented in [5] has been selected for interface capturing. In this method [17, 5], the interface is implicitly represented by a regularized indicator function ϕ:

$$\phi(\mathbf{x}, t) = \frac{1}{2}\left(\tanh\left(\frac{d(\mathbf{x}, t)}{2\varepsilon}\right) + 1\right) \tag{3}$$

where ε is a parameter for controlling the thickness of the interface. The fluid interface can be located by getting the $\phi = 0.5$ isosurface. Based on this function, the density and viscosity of the fluid are computed as follows:

$$\rho = \rho_1 \phi + \rho_2 (1 - \phi) \tag{4}$$

$$\mu = \mu_1 \phi + \mu_2 (1 - \phi) \tag{5}$$

The level set function is advected by the velocity field, solution of the Navier-Stokes equations:

$$\frac{\partial \phi}{\partial t} + \nabla \cdot \phi \mathbf{v} = 0 \tag{6}$$

Furthermore, an additional re-initialization equation is introduced to keep constant the thickness of the interface [18]:

$$\frac{\partial \phi}{\partial \tau} + \nabla \cdot \phi (1 - \phi) \mathbf{n}_{\tau=0} = \nabla \cdot \varepsilon \nabla \phi \tag{7}$$

where τ is the pseudo-time. This equation consist of a compressive term $\phi (1 - \phi) \mathbf{n}_{\tau=0}$ to sharpening the profile, and a diffusion term $\nabla \cdot \varepsilon \nabla \phi$, that ensure the profile remains of characteristic thickness ε.

By using the CSF method developed by Brackbill et al. [19] two issues can be handled: the computation of the curvature κ and the application of the resulting pressure jump to the fluids. Therefore, the singular term $\sigma \kappa \mathbf{n} \delta_\Gamma$ is converted to a volume force as follows:

$$\sigma \kappa \mathbf{n} \delta_\Gamma = \sigma \kappa (\phi) \nabla \phi \tag{8}$$

where $\mathbf{n}$ and $\kappa (\phi)$ are given by:

$$\mathbf{n} = \frac{\nabla \phi}{\| \nabla \phi \|} \tag{9}$$

$$\kappa (\phi) = -\nabla \cdot \mathbf{n} \tag{10}$$

Here, $\nabla \phi$ is evaluated by using the least-square method [5]. The reader is referred to [5] for technical details on the finite-volume discretization of the governing equations.

2.1. Time step

A CFL condition limits the time step for stable calculations. By a trivial comparison among the terms of equation 1, the different characteristics time steps shown in table 1 are obtained. The global time step should be smaller than each of them.

Table 1. Time step conditionals for the proposed method, where $(\Delta t)_{\text{conv}}$ is the convective time step, $(\Delta t)_{\text{visc}}$ is the viscous time step, $(\Delta t)_{\text{g}}$ is the gravity time step, $(\Delta t)_{\text{cap}}$ is the time step due to the surface tension source, and $(\Delta t)_{\text{mesh}}$ is the time step due to the characteristic mesh velocity. Subscript n denotes that the corresponding variable is evaluated at the node n under consideration, and Δ_n is the characteristic size of the control volume n calculated as the cubic root of the cell volume.

$(\Delta t)_{\text{conv}}$	$(\Delta t)_{\text{visc}}$	$(\Delta t)_{\text{g}}$	$(\Delta t)_{\text{cap}}$	$(\Delta t)_{\text{mesh}}$
$\min\left(\frac{\Delta_n}{\|\mathbf{v}_n\|}\right)$	$\min\left(\frac{\Delta_n^2 \rho_n}{\mu_n}\right)$	$\sqrt{\min\left(\frac{\Delta_n}{\|\mathbf{g}\|}\right)}$	$\min\left(\left(\frac{\rho_1+\rho_2}{4\pi\sigma}\right)^{1/2} (\Delta_n)^{3/2}\right)$	$\min\left(\frac{\Delta_n}{\|\mathbf{v}_{mesh}\|}\right)$

2.2. Calculation algorithm
The process carried out in order to advance from the current time step t^m to the following one t^{m+1} is summarized as follows:

(i) Obtain the mesh velocity by computing the bubble velocity.
(ii) Compute the time step (see section 2.1).
(iii) Advect the conservative level set function ϕ, by solving equation 6.
(iv) Solve re-initialization equation 7.
(v) Density, viscosity and curvature fields are updated from the level set field.
(vi) Solve the Navier-Stokes equations by using the fractional step method [20]:
  – Calculate the predictor velocity.
  – Solve the Poisson equation to get the pressure field.
  – Calculate the final velocity.
(vii) Move the mesh.

The previous steps should be repeated up to the desired time.

3. Three dimensional Taylor bubble
Once the method has been described, the full three dimensional Taylor bubble problem is addressed. Results have been compared against those of Bugg and Saad [12] and Ndinisa et al. [13].

3.1. Setting-up
Figure 2 shows the initial set up for the tested case. The simulation is based on the conditions described by Ndinisa et al. [13]. The density of the continuous phase ρ_1 is 911kg/m^3, and its viscosity μ_1 is 0.084Pa $\cdot$ s. The properties of the bubble's fluid are $\rho_2 = 1.205$kg/m^3 and $\mu_2 = 1.827 \cdot 10^{-5}$Pa $\cdot$ s. The surface tension coefficient σ is 0.0328N/m. The pipe's diameter D is 0.019m. The bubble's length h_b is 0.0523m and its radius $r_0 = 0.007$m. The aforementioned conditions give rise to the following dimensionless groups: $Eo = \rho_1 g D^2/\sigma = 100$, $Mo = g\mu_1^4/\left(\rho_1\sigma^3\right) = 0.015$, $\eta_\rho = \rho_1/\rho_2 = 756.017$ and $\eta_\mu = \mu_1/\mu_2 = 4597.701$. The expected terminal Reynolds number $Re_T = \rho_1 U_T d/\mu_1$ is about 27, where U_T is the terminal velocity. Non-slip boundary condition is applied at the lateral walls. A zero-velocity inlet boundary condition is imposed at the top of the domain and an outlet boundary condition at its bottom. The formulation of the employed outflow boundary condition is explained in [21]. For technical details about the numerical treatment of the equations, the reader is referred to [5].

3.2. Mesh configuration
The mesh has cylindrical shape and it is made up of hexahedral control volumes uniformly distributed. Figure 3 depicts a sketch of this mesh. It was generated by a constant step extrusion of a plane grid along the cylinder axis. Table 2 describes the three considered (namely, $M1$, $M2$ and $M3$).

The distance from the bubble centroid to the inflow h_i is set to $2D$. Upstream perturbations do not propagate beyond $0.5D$ from the bubble nose (see figure 6), so a distance of $2D$ to the inlet is enough. Additionally, distance to the outlet h_o is set to $3D$, since it gave rise to enough accurate stability in preliminary simulations. Therefore, the total axial distance y_{length} is $5D$. This considerably reduces the domain size compared to other works (see for instance [4]).

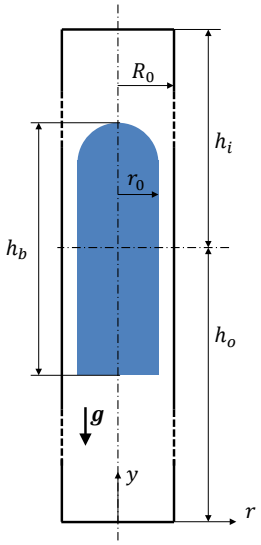

Figure 2. Initial set-up of the Taylor bubble problem.

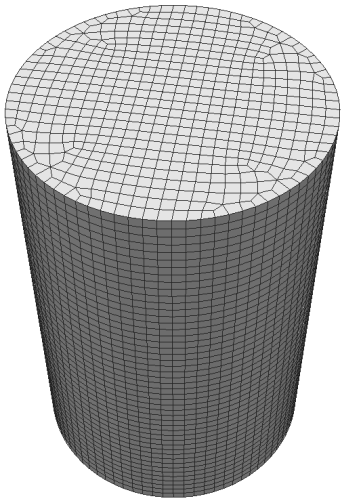

Figure 3. Mesh configuration for the Taylor bubble problem.

Table 2. Description of the meshes used in the Taylor bubble problem.

Mesh name	Mesh size	Cells per plane	N_{planes}	y_{length}	h_{char}
$M1$	$5.3 \cdot 10^5$	2098	254	$5D$	$D/52$
$M2$	$1.9 \cdot 10^6$	5043	380	$5D$	$D/76$
$M3$	$3.7 \cdot 10^6$	7891	475	$5D$	$D/95$

3.3. Time evolution

The evolution of the Reynolds number Re along the dimensionless time t^* is shown in figure 4. Moreover, table 3 summarizes the obtained results, comparing them against the ones obtained by other authors, and showing a good agreement when $M2$ and $M3$ meshes are used. With $M1$ mesh, results are not enough accurate. Additionally, figure 5 sketches the bubble shape evolution along the time.

Table 3. Results of the Taylor bubble problem, where E_{U_T} is the relative error compared to the experimental results of Bugg and Saad [12].

Case	U_T	E_{U_T}
Present work ($M1$)	0.1210m/s	7.63%
Present work ($M2$)	0.1277m/s	2.52%
Present work ($M3$)	0.1286m/s	1.83%
Ndinisa et al. [13]	0.140m/s	6.87%
White and Beardmore [2]	0.1272m/s	2.90%
Bugg and Saad [12]	0.131m/s	—

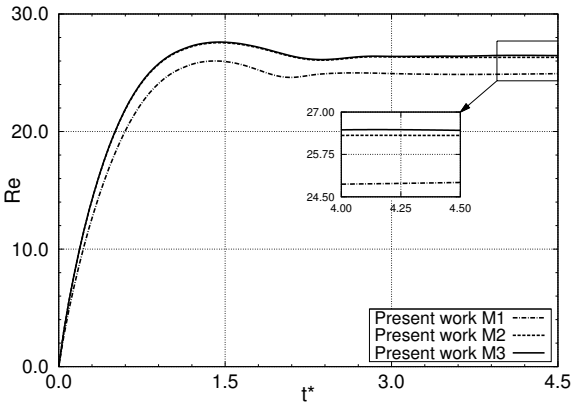

Figure 4. Velocity evolution (in m/s) of the tested Taylor bubble.

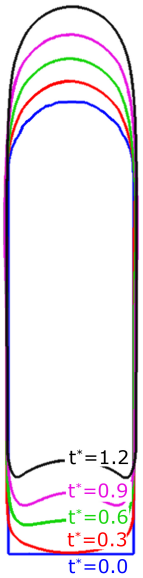

Figure 5. Profiles evolution of the tested Taylor bubble when $M3$ mesh is used.

3.4. Results discussion

Figures 6 to 9 show different velocity profiles plotted over several sections of the bubble, and the comparison against the reference data. These results are represented for the three considered meshes. Furthermore, velocity field and the streamlines are depicted in figures 10 to 12. By analyzing these results, an accurate description of the velocity field is obtained.

First, figure 6 shows the the normalized axial velocity along the tube axis above the bubble. The ascent of the buoyant bubble induces perturbations above it. However, these disturbances do not propagate more than $D/3$ above the bubble nose, as seen in the aforementioned figured. Nearby the bubble nose, the fluid is essentially radial, due to the fact that the Taylor bubble is moving upwards and the continuous phase ahead of it is been pushed sideways. This issue can be appreciated in figure 7, where the normalized radial velocity across the tube radius at $0.111D$ above the bubble nose is plotted. For its part, figure 8 shows the normalized radial velocity in the developing film at $0.504D$ below the bubble nose. As can be seen in this figure, a strong radial velocity component is still observed when descending into the developing film, especially in the vicinity of the bubble's interface. The developing film thins as it progresses, and the fluid velocity rises. Then, when the fully developed film is formed, an essentially axial and constant flow can be observed. When the rear end is achieved, the axial velocity is drastically reduced. This is illustrated in figure 9, where the normalized axial velocity at $0.2D$ below the bubble's rear end is plotted. Below this point, the flow becomes strongly radial.

Results are compared against the experimental data of Bugg and Saad [12] and the numerical study of Ndinisa et al. [13]. When $M2$ and $M3$ meshes are used, results are in good agreement. In contrast, the $M1$ mesh does not seem enough fine to accurate solve the problem.

The streamlines and velocity field depicted in figures 10, 11 and 12 agree qualitatively with the results published in [12] and [13]. As may be seen from these images, the problem is fundamentally axisymmetric. Moreover, two large counter rotating vortices are observed inside the Taylor bubble. No vortex appears in the wake of the bubble.

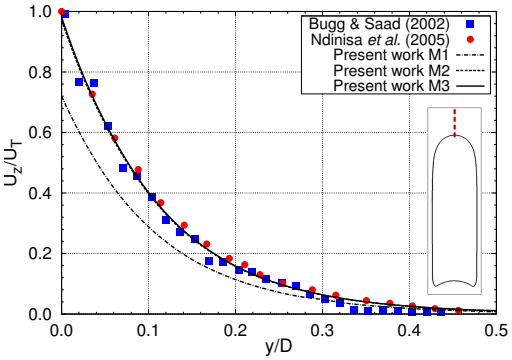

Figure 6. Normalized axial velocity along the tube axis above the bubble nose.

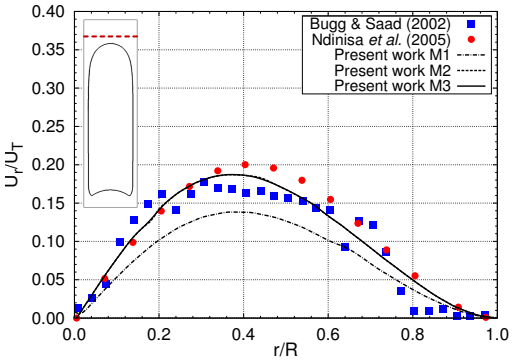

Figure 7. Normalized radial velocity across the tube radius at $0.111D$ above the bubble nose.

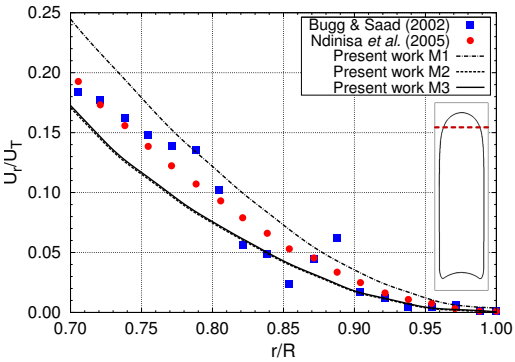

Figure 8. Normalized radial velocity in the developing film at $0.504D$ below the bubble nose.

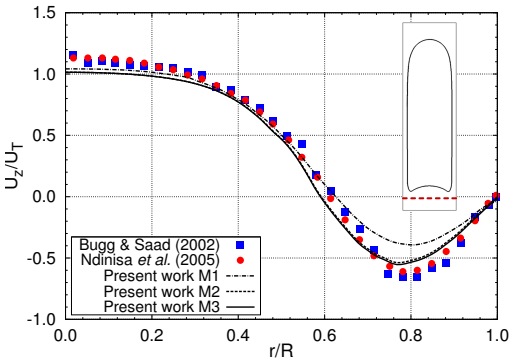

Figure 9. Normalized axial velocity in the wake of the bubble at $0.2D$ below the bubble.

4. Conclusions

In the present work the challenging problem of the three dimensional Taylor bubble has been studied. On the one hand, a Conservative Level Set formulation was chosen to deal with the multiphase flow domain. On the other hand, a moving mesh method was used as domain optimization technique. By using an optimized domain, the efficiency of the simulation can be notably improved, due to the fact that it is no longer necessary to solve regions far from the vicinity of the bubble. Once the method has been formulated, the full three dimensional Taylor bubble problem was addressed, without the axisymmetric assumption. Results have been compared against those of Bugg and Saad [12] and Ndinisa et al. [13]. Detailed descriptions of the velocity field, shape evolution and terminal velocity were provided, showing a good agreement in comparison with the reference data.

Acknowledgments

This work has been financially supported by the *Ministerio de Economía y Competitividad, Secretaría de Estado de Investigación, Desarrollo e Innovación* of Spain (Project VAPFLOW, ENE-2012-36910). and by Termo Fluids S.L.

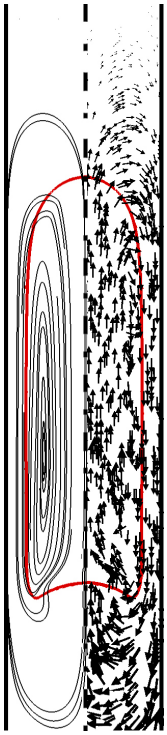

Figure 10. Streamlines and velocity field of the Taylor bubble problem.

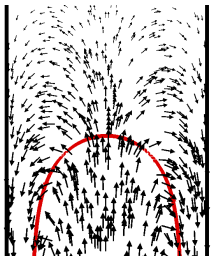

Figure 11. Velocity field detail at the nose of the Taylor bubble.

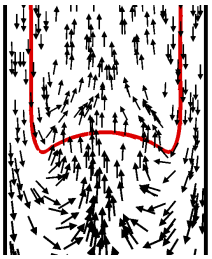

Figure 12. Velocity field detail at the rear end of the Taylor bubble.

References

[1] Davies R M and Taylor G 1950 *Proc. R. Soc. A Math. Phys. Eng. Sci.* **200** 375–390
[2] White E and Beardmore R 1962 *Chem. Eng. Sci.* **17** 351–361
[3] E Shosho C and E Ryan M 2001 *Chem. Eng. Sci.* **56** 2191–2204
[4] Quan S 2011 *Int. J. Multiph. Flow* **37** 888–897 ISSN 03019322
[5] Balcázar N, Jofre L, Lehmkuhl O, Castro J and Rigola J 2014 *Int. J. Multiph. Flow* **64** 55–72
[6] Gaudlitz D and Adams N 2009 *Phys. Fluids* **21** 1–9
[7] Schlatter P, Adams N and Kleiser L 2005 *J. Comput. Phys.* **206** 505–535
[8] Rusche H 2002 *PhD thesis*
[9] Ruzicka M C 2000 *Int. J. Multiph. Flow* **26** 1141–1181
[10] Estruch O, Lehmkuhl O, Borrell R, Segarra C D P and Oliva A 2013 *Comput. Fluids* **80** 44–54
[11] Marschall H, Boden S, Lehrenfeld C, Falconi D, Carlos J, Hampel U, Reusken A, Wörner M and Bothe D 2013 *Comput. FLUIDS* **102** 1–21
[12] Bugg J D and Saad G A 2002 *Int. J. Multiph. Flow* **28** 791–803
[13] Ndinisa N V, Wiley D E and Fletcher D F 2005 *Chem. Eng. Res. Des.* **83** 40–49
[14] Balcázar N, Lehmkuhl O, Jofre L and Oliva A 2015 *Int. J. Heat Fluid Flow* **56** 91–107
[15] Balcázar N, Lehmkuhl O, Rigola J and Oliva A 2015 *Int. J. Multiph. Flow* **74** 125–142
[16] Tryggvason G, Bunner B, Esmaeeli A, Juric D, Al-Rawahi N, Tauber W, Han J, Nas S and Jan Y J 2001 *J. Comput. Phys.* **169** 708–759
[17] Olsson E and Kreiss G 2005 *J. Comput. Phys.* **210** 225–246 ISSN 00219991
[18] Harten A 1978 **32** 363–389
[19] Brackbill J, Kothe D and Zemach C 1992 *J. Comput. Phys.* **100** 335–354
[20] Guermond J L, Minev P and Shen J 2006 *Comput. Methods Appl. Mech. Eng.* **195** 6011–6045
[21] Davis R W and Moore E F 1982 *J. Fluid Mech.* **116** 475